View metadata, citation and similar papers at core.ac.uk
brought to you by CORE
provided by Apollo

13th January, 2015

Magnetic resonance imaging of gas dynamics in the freeboard of fixed beds and bubbling fluidized beds

C. M. Boyce*†, N. P. Rice, J. F. Davidson, A. J. Sederman,
J. S. Dennis, D. J. Holland‡

Department of Chemical Engineering and Biotechnology, University of Cambridge, New Museums Site, Pembroke Street, Cambridge CB2 3RA, UK.

(*) Corresponding author. Email: cmboyce@princeton.edu. Tel: +1-646-255-4807
(†) Current address: Department of Chemical and Biological Engineering, Princeton University, Princeton, NJ 08544
(‡) Current address: Department of Chemical and Process Engineering, University of Canterbury

Abstract

Magnetic resonance imaging (MRI) was used to measure directly gas velocity and gas velocity distribution in the freeboard region of a fluidized bed (52 mm dia.) under bubbling fluidization and just below minimum fluidization. The bed consisted of poppy seed particles 1.1 mm in diameter and was fluidized using SF_6 gas at 7.5 barg for MRI purposes. In the system, bubbles approximately 20 mm in diameter rose through the centre of the bed. In the case of bubbling fluidization, time-averaged velocity maps at different vertical positions in the freeboard showed downward moving gas in the centre of the bed and upward moving gas near the walls for this particular bed. However, below minimum fluidization conditions, the profiles of gas velocity in the freeboard were flat, with respect to the radial dimension, with minor and random spatial variance, indicating that the profiles observed during bubbling arose from bubble breakthrough. The reasons for these observed patterns of flow are discussed.

Keywords: fluidized beds; freeboard; magnetic resonance imaging; flow measurement

1. Introduction

Gas flow patterns in the freeboard region above the particles in a fluidized bed are important practically, since they strongly influence the elutriation of fine particles. Additionally, the patterns of mixing are important where gaseous reactions occur in the freeboard, *e.g.* the reaction of volatile matter escaping to the freeboard during the combustion of coal or biomass. Experiments have shown that gas flow patterns in the freeboard are related to the release of gas from bubbles breaking through the upper surface of the fluidized bed (Levy and Lockwood, n.d.; Pemberton and Davidson, 1984).

Three theories have emerged to describe the relationship between gas flow patterns in the freeboard and bubble breakthrough. These are: (a) the pulsed jet theory (Zenz and Weil, 1958), (b) the "ghost bubble" theory (Pemberton and Davidson, 1984), and (c) the toroidal vortex theory (Levy and Lockwood, 1983). Zenz and Weil (Zenz and Weil, 1958) proposed that the eruptions of bubbles would lead to periodic, jet-like pulses of gas coming from the top of the bed into the freeboard. Using hot-wire anemometry, Pemberton and Davidson (Pemberton and Davidson, 1984) proposed that a "ghost bubble" is formed after bubble breakthrough, with the gas from the bubble staying largely intact after eruption, and maintaining its original circulation pattern as it rises up the freeboard. Using laser Doppler anemometry (LDA), Levy and Lockwood (Levy and Lockwood, 1983) proposed a mechanism in which a toroidal vortex of gas flow is formed after the breakthrough of a bubble. This toroidal vortex then rises steadily up the freeboard with the bulk flow of the gas. This theory was confirmed by measurements at a variety of points in the freeboard, as well as later measurements using planar laser induced fluorescence (PLIF) (Hartung et al., 2008; Müller et al., 2009; Solimene et al., 2007) and particle image velocimetry (PIV) (Duursma et al., 2001; Yórquez-Ramírez and Duursma, 2001).

As noted above, previous research for determining gas flow patterns in fluidized beds has used a variety of measuring techniques, most requiring an intrusion into the system under study. Here, magnetic resonance imaging (MRI) was used to measure gas velocity directly and non-intrusively in a 3D cylindrical fluidized bed. MRI is capable of measuring gas velocity and velocity distribution in a spatially-resolved manner without any intrusion into the bed. However, the main limitations of the MRI measurements used here were that only time-averaged measurements were possible and the diameter of the bed (52 mm) was small, being limited by the diameter of the bore of the available magnet and radiofrequency coil. Also, the particle diameter used (~1 mm) was somewhat larger than that used in many industrial-scale fluidized bed reactors. Measurements of the velocity of the gas, at various positions in the freeboard, were made under both bubbling and fixed bed conditions. This work was part of a greater body of work to develop the MRI techniques necessary to measure gas velocities within fluidized beds (Boyce et al., 2015b).

2. Experimental

2.1 Fluidized bed

Table 1 summarises the principal parameters of the fluidized bed arrangement. The bed had a diameter D_{bed} = 52 mm. It was filled with poppy seeds, with diameter d_p = 1.1 mm, to a tapped bed height of H_0 = 100 mm. These particles were used because they could be detected using magnetic resonance to enable assessment of the bubble size in the system. Gaseous SF_6 at 7.5 barg was used to fluidize the particles, because this gas could be detected in magnetic resonance imaging (MRI) by means of the ^{19}F nuclei. The bed of particles was supported on a porous sintered bronze plate, which was used as a distributor. The plenum chamber was filled with glass beads approximately 2 mm in diameter to assist with even distribution of the gas. The

pressure drop across the distributor was measured to be ~10 mbar at minimum fluidization, which is greater than the pressure drop across the bed of ~6 mbar. In addition, spatially-resolved maps of gas velocity near the distributor showed an even distribution of gas.

The minimum fluidization velocity for these particles in SF_6 gas at 7.5 barg was measured using both pressure and MRI to be U_{mf} = 0.090 ± 0.002 m/s. The classifications of Geldart (Geldart, 1973) as well as those of Grace (Grace, 1986) and Yang (Yang, 2007) all categorise the combination of gas and particles used here as Group D, meaning that bubbling could be expected immediately after reaching the minimum fluidization velocity, U_{mf}. Observation of bubbling using MRI showed that bubbling occurred at superficial velocities directly above U_{mf}.

A Bronkhorst F-113AC-M50-AAD-55-E mass flow controller, designed and calibrated for SF_6, was used to control gas flow. The accuracy of the mass flow controller was ±0.5%, assuring accuracy in the superficial velocities at which the experiments were conducted.

2.2 MRI arrangement

The MRI arrangement was identical to that described elsewhere (Boyce et al., 2015b). MRI measurements were conducted using a Bruker DMX 200 spectrometer with a magnetic field strength of 4.7 T. The magnet was operated at a proton (^{1}H) frequency of 199.7 MHz to measure signal from the oil in the poppy seeds and a ^{19}F frequency of 187.9 MHz to measure signal from the SF_6. This separation of frequencies allowed signal from the particles and gas to be measured separately without interference between them. A birdcage radiofrequency (r.f.) coil (capable of tuning to either the ^{1}H or the ^{19}F frequency) with an inner diameter of 64 mm was situated around the fluidized bed to excite and detect signal from the seeds and gas. A shielded 3-

axis gradient set capable of producing a maximum gradient of 0.139 T/m was used for imaging and velocimetry.

The magnetic field was not entirely homogenous because of (1) a severed connection to the cryogenic shim set and (2) interference from the stray field of another MRI magnet in the same room. Thus, various efforts were made to ensure the measurements were as accurate as possible, as follow. (a) No imaging was conducted with slices in the vertical plane because the magnetic field was more heterogeneous in the vertical direction than in the horizontal direction. (b) All measurements were obtained using slice selection such that signal was only obtained from a narrow, horizontal slice through the bed. (c) The magnetic field was shimmed on the slice, rather than a full excitation of the material in the r.f. coil, as there could be significant differences in the shim necessary for the slice. (d) Two-dimensional imaging used phase encoding only, because the signal attenuation was too rapid (T_1 = 20 ms; T_2 = 13 ms; T_2^* = 0.5 ms) to support accurate use of a read gradient during the FID. (e) All measurements were conducted in the centre of the r.f. coil, and the fluidized bed was moved up and down to investigate different regions of the bed because the magnetic field was most homogenous in the region aligned with the centre of the r.f. coil. With these restrictions, high quality, quantitative images were obtained, as demonstrated in the results section, as well as in other work (Boyce et al., 2015a, 2015b).

2.3 Spatial maps of time-averaged gas velocity

Maps of time-averaged gas velocity in the vertical direction were acquired in the bed of particles as well as in the freeboard using an 11-interval MRI pulse sequence (Boyce et al., 2015b). Parameters for these measurements are summarised in Table 2. The experimental determinations of gas velocity were obtained using a circular sampling of 193 points on a 16 by

16 Cartesian grid in *k*-space. The circular sampling was used because it allows for a 25% reduction in acquisition time without losing a significant amount of signal intensity or sharpness of the circular image in real space. Four averages of this sampling in *k*-space were obtained, making the acquisition time approximately 40 minutes per image. MRI measurements were made under conditions of bubbling fluidization with a superficial velocity U = 0.104 m/s and at U = 0.080 m/s, just below minimum fluidization. These measurements were made at a variety of positions in the freeboard, as shown in Table 3. The maximum expanded bed heights for U = 0.104 m/s and 0.080 m/s were, respectively, H = 120 mm and 113 mm. Determinations of gas velocity were only made for the vertical (z) component of the velocity, because images for the horizontal components of the gas velocity showed interference with the imaging gradients, and hence quantitative maps of velocity in the *x*- and *y*-directions were not possible.

2.4 Measurements of gas velocity distribution

Velocity distributions of SF_6 gas were acquired at different superficial velocities and different positions in the freeboard using propagator measurements. Propagator measurements are a magnetic resonance technique similar to velocity measurements, but they use a number of small increments in the magnitude of the flow encoding gradient to determine a distribution of velocities rather than an average velocity (Callaghan, 1991). Also, although it was not possible to determine the velocities in the horizontal directions using the technique in Section 2.3, it was possible to do so using propagator measurements. Propagator measurements are not images and so do not require the use of imaging gradients. Therefore, measurements of the horizontal components of the velocity were possible without any interference between the flow encoding gradients and imaging gradients. Thus, the distributions of the horizontal components of the velocities were measured for the entire cross-section of the freeboard at a particular height, *z*,

above the bed surface, with a slice thickness in the vertical direction of 4 mm. The propagator measurements used the 11-interval pulse sequence with the parameters summarised in Table 4. For the propagator measurements, all three components of the velocity were measured.

3. Results

Maps of the vertical component of the gas velocity were obtained at various positions above the bed at superficial velocities of U = 0.080 m/s and U = 0.104 m/s, with the bed just below minimum fluidization and bubbling at the respective flow rates. Table 5 shows the average gas velocities obtained from averaging the velocities in the pixels of velocity maps at the various positions and flow rates. From this Table, the important conclusion can be drawn that there is excellent agreement between the superficial velocity, as determined by the mass flow rate of SF_6 into the apparatus, and the average velocity determined by magnetic resonance measurements of the gas. This agreement, therefore, is confirmation that MR can be used to make measurements on the gas phase, in addition to previous work showing that it is an effective technique for imaging the solids in fluidized beds (Holland et al., 2008). In Table 5, the error in the average velocity measured by MRI was ±0.002 m/s, based on three repetitions of the measurement. The error in the expected velocity arises from the errors in the temperature, pressure, and mass flow rate. On the basis of these, the overall error was estimated to be ±0.002 m/s. As seen in Table 5, the average velocity measured by MRI agreed with the average velocity determined by the flow meter to within the estimated experimental error for all cases.

Figure 1 (I-VI) shows maps of the vertical component of the time-averaged velocity of the gas at different vertical positions in the freeboard above the expanded bed height. Figure 1 (a-f) shows the plots of the values of time-averaged velocities from a central slice through the maps in (I-VI). For these measurements the bed was in a state of bubbling fluidization, and the

Reynolds number, based on the open-tube, superficial flow in the reactor, was $Re = (D_{bed}\rho_g U)/\mu = 18{,}900$. The error in the measured velocity in any given pixel was estimated to be ±0.01 m/s, on the basis of the apparent noise level in the raw measurements. Under these flow conditions, the expanded bed height was H = 120 mm. At $z - H$ = 10 mm in Figure 1 (I), the local time-averaged velocity is downwards in the centre of the bed, reaching U_z = -0.03 m/s; the velocity increases with distance from the centre of the map in Figure 1(I) to velocities above 0.20 m/s. This axially-symmetric pattern is also seen in the maps in Figures 1 (II)-(V), but the profiles become flatter with increasing $z - H$, with the velocity increasing in the centre of the bed and decreasing near the walls. At $z - H$ = 90 mm in Figure 1 (V), the flow profile is nearly uniform with velocities as low as 0.08 m/s in a central region and as high as 0.13 m/s in an annular region near the walls. At $z - H$ = 180 mm in Figure 1 (VI), the velocity profile is fairly flat with velocities in the centre of the bed slightly higher than those adjacent to the walls, consistent with the formation of a turbulent flow profile.

Figure 2 shows maps of the velocity of the gas in the freeboard when the bed is held at U = 0.080 m/s, just below minimum fluidization (U_{mf} = 0.090 m/s). In this case the variations in velocity from pixel to pixel are smaller and more random spatially than with the bubbling case shown in Figure 1. Figure 2(a) shows a distribution of velocities in the fixed bed case at $z - H$ = 10 mm; it manifests the largest variance in velocities of all the cases of the fixed state and apparently random variations from one pixel to the next. With increasing values of $z - H$, the variations become smaller and larger regions of connected pixels are observed. At H = 180 mm above the expanded bed height (d), a fairly flat velocity profile is seen with slightly lower velocities near the walls, consistent with a turbulent flow profile. To conclude, the results of Figures 1 and 2 suggest that once the bed is in a bubbling state, an ordering of flow in the

freeboard is seen, with higher vertical velocities of flow near the walls for points within ~50 mm above the maximum height of the fluidized bed.

To examine in further detail the distributions of velocity in the freeboard of the bubbling fluidized bed, it is first necessary to examine the bubbling pattern by imaging the gas *within* the bed. Figure 3 shows time-averaged maps of the vertical component of gas velocity within the bed. For z = 25-100 mm above the distributor in Figures 3(B)-(E), there is a profile of fast upward-moving velocities, of up to 0.7 m/s, in the centre of the bed, and a profile of much lower, upward-moving velocities, ~0.15 m/s, in a larger outer annulus of pixels. This suggests a stream of bubbles rising axially with a diameter ~20 mm. Close to the distributor, Figure 3(A), a wider central profile shows gas velocities ~ 0.25 m/s while an outer annulus has gas velocities around 0.1 m/s. At the expanded bed height in Figure 3(F), the profile appears relatively uniform across the cross-section of the bed with time-averaged gas velocities in the pixels around 0.15 m/s. Upon closer inspection of Figure 3 (F), there is an annular ring of diameter ~30 mm in which the gas velocity is ~0.12 m/s, whilst in the centre of the bed and at the walls the velocity is ~0.17 m/s, i.e. somewhat higher than in the annular ring; the difference is difficult to resolve here as the colour scale was optimised for the images within the bed and not the freeboard region. To summarize, the maps in Figure 3 are consistent with a train of bubbles approximately 20 mm in diameter rising and erupting exclusively in the centre of the bed; this pattern is further confirmed by MRI measurements of void fraction and particle velocity, shown elsewhere (Boyce et al., 2015a).

Figure 4 shows distributions of horizontal components of gas velocity, along a particular horizontal (y) direction, produced from propagator measurements at different vertical positions above the expanded bed height in the freeboard. Horizontal components of velocity for velocities

not parallel to the *y*-axis have been resolved parallel to the *y*-direction before being shown in the Figure. The measurements shown in Figure 4 can be considered to be probability distribution functions of the horizontal *y*-component of the velocity at each height. Roughly speaking, at $z - H = 10$ mm the distribution is broad, reaching velocities as high as 0.25 m/s and as low as -0.25 m/s. With increasing distance above the expanded bed height, the distributions become narrower. In all cases, the distributions are symmetric, with a modal velocity of 0 m/s. The error for the results in Figure 4 is indicated by the random scatter in the baseline of the curves; the random scatter is < 1% for all curves and thus is small. At a height of $z - H = 180$ mm, the width of the velocity distribution is of the order of the resolution of the measurement, 0.0625 m/s (see Figure 4). The probability distribution is obtained from a discrete Fourier transform of the measurements. For measurements where the width of the distribution is comparable to the resolution, an additional systematic artefact arises from the truncation of the discrete Fourier transform. This artefact causes the unphysical negative probability observed at velocities of ±0.12 m/s.

Figure 5 is similar to Figure 4, showing distributions of all the horizontal components of gas velocity, along a particular horizontal (*y*) direction produced from propagator measurements at $z - H = 10$ mm in the freeboard for different superficial velocities. In the case of zero flow, with the reactor full of SF_6 and the flow turned off, the gas velocity distribution is narrow, but is far from the ideal expected (a Dirac function at a gas velocity of zero). The apparent velocity distribution observed in this experiment arises from the diffusive motion of the gas molecules, and any convective flow arising from temperature differences along the length of the tube. Accordingly, the width of the distribution for zero gas velocity can be used as an indication of the limit of detection of the probability distribution for the velocity arising from flow. When the

superficial velocity was increased to U = 0.080 m/s, just below U_{mf}, the distribution of gas velocities becomes only slightly broader. In contrast, a small further increase in superficial gas velocity to U = 0.104 m/s, corresponding to bubbling fluidization, gives a distribution of gas velocities that is significantly broader, confirming the influence of bubbling on freeboard behaviour noted in Figure 1.

4. Discussion

It is important to consider the results presented above in the light of published theories for gas flow in the freeboard. The velocity maps in the bed of particles suggest that bubbles ~20 mm in diameter travel up through the centre of the bed with few bubbles appearing at the walls, if any. In the freeboard when the bed is undergoing bubbling fluidization, the velocity of the gas is low in the centre of the bed and high at the walls, with the difference in velocity decreasing with increasing height above the top surface of the bed (see Figure 1).

The pulsed jet theory (Zenz and Weil, 1958) suggests that bubbles generate a high gas velocity at the point of eruption. In this fluidized bed, the lowest gas velocities are seen at the point of bubble eruption, as shown in Figure 1 (a). Therefore, the results presented here are not consistent with the pulsed jet theory of gas flow in the freeboard. However, it is important to note that the diameter of this bed is 52 mm, and the bubbles were largely confined to forming on the axis of the bed. It is therefore possible that the pulsed-jet theory could hold in a larger bed in which bubbles erupt at different horizontal positions in the bed and multiple bubbles can erupt at once.

The ghost bubble theory suggests that the gas flow patterns present in bubbles within the bed of particles are maintained above the top of the bed in the freeboard. Standard theory (Davidson, 1961) and the measurements in Figure 3 show that gas travels fastest upwards

through bubbles and more slowly through the interstices between particles. Thus, the ghost bubble theory predicts that the gas velocities would be fastest in the centre of the freeboard and slower near the walls. The results presented above indicate that the gas velocity is high at the walls and low in the centre of the bed. This is almost the inverse of the gas flow pattern expected from the ghost bubble theory. There are several possible explanations for this discrepancy. Firstly, it is possible that the flow pattern seen here is influenced by the walls of the column, as the column is only 52 mm in diameter. However, similar findings have been reported in larger beds using laser-based techniques (Duursma et al., 2001; Hartung et al., 2008; Müller et al., 2009; Solimene et al., 2007; Yórquez-Ramírez and Duursma, 2001). Secondly, the measurements reported here are a time-averaged measurement. It is possible that the bubble eruption pattern produces a bulk flow that is shaped as measured here, but fluctuations may arise along the centre-line of the bed owing to ghost bubbles. If the fluctuations in the velocity were much greater along the centre-line of the bed than at the walls, then the MRI measurements should indicate this by a decrease in the signal intensity in the centre of the bed (Callaghan, 1991). A decrease in the intensity in the centre of the bed was not observed in the images, therefore the intensity of fluctuations at the wall and along the centre-line of the bed is likely to be similar in magnitude.

The third model for gas flow in the freeboard considered here is the toroidal vortex theory of Levy and Lockwood (Levy and Lockwood, 1983). The basis of this theory is shown schematically in Figure 6. Upon a bubble breaking through the surface of the bed, there is initially an upward movement of gas as it is released into the freeboard (Figure 6a ii). The particles from the crown of the bubble are initially ejected but then fall back to the surface of the bed. As these particles fall back on to the top surface of the bed, they exert a drag on the gas

which causes the direction of the gas flow to reverse and hence the gas flows downwards along with the particles (Figure 6a iii). Continuity means that this downward flow of gas must be balanced by an upward flow of gas elsewhere in the bed, typically at the walls. In a freely bubbling bed, this gas flow pattern is thought to give rise to a toroidal vortex with, on average, downward flow of gas in the centre and upward flow at the walls. The central cross-section of this toroidal vortex is illustrated in Figure 6 (b). The general toroidal flow pattern will also exhibit significant fluctuations in velocity or turbulence. The toroidal vortex rises with the main gas flow, decaying with distance above the bed, most probably owing to inertial effects.

The flow pattern observed in our measurements in the freeboard of the bubbling bed showed very slow or even downwards flow in the centre of the bed with fast upward flow at the walls (Figure 1). The gas velocity at the walls was observed to decrease with increasing height above the top surface of the bed, eventually reaching a flow profile consistent with turbulent flow, as expected given the Reynolds number based on the open tube was 18,900. This gas flow pattern is consistent with the toroidal vortex model of gas flow in the freeboard. The toroidal gas flow pattern is directly connected with the formation of bubbles because no toroidal flow was observed for flow just below minimum fluidization (Figure 2). The distributions of the *y*-component of the velocity shown in Figure 4 are also consistent with the toroidal vortex theory, since the velocity distribution becomes more uniform with distance above the expanded bed height, characteristic of a decaying toroidal vortex. Additionally, the comparison of the distributions of the *y*-component of the velocity at different superficial velocities in Figure 5 shows a much broader velocity distribution in the bubbling regime, characteristic of a new flow pattern emerging due to the onset of bubbling.

Similar observations of high flow at the walls of the bed and low or downward flow in the centre of the bed have been made in the original paper using laser Doppler anemometry (Levy and Lockwood, 1983), as well as particle image velocimetry (PIV) and planar laser induced fluorescence (PLIF) measurements (Duursma et al., 2001; Hartung et al., 2008; Müller et al., 2009; Solimene et al., 2007; Yórquez-Ramírez and Duursma, 2001).

The presence of a decaying toroidal vortex and ultimate transition to turbulent flow at $z - H$ = 180 mm in Figure 1 presents an interesting "entry-length" problem in single phase flow. After the toroidal vortex is formed, the viscous shear of the gas phase, combined with inertial effects, leads to decay of the vortex with height, eventually leading to fully-developed pipe flow. Owing to the importance of gas flow patterns in the freeboard region for combustion reactions and particle elutriation, this issue suggests the need to characterise the "entry length" for the transition to fully developed flow above the expanded bed height. Our preliminary measurements on this matter indicate that by 180 mm above the expanded bed height, the flow is approaching the classical $1/7^{th}$ power fit to a turbulent velocity profile. Thus, the flow was close to fully developed at an entrance length of $z - H$ = 90-180 mm in this system, or 2-4 bed diameters. This entry length is significantly less than the 10 pipe diameter entry length typically used to give fully developed turbulent flow in pipes. It is possible that this entry length problem is more directly correlated with the diameter of bubbles, rather than the diameter of the bed, since the entry length is likely related to the initial size of the toroidal vortex which is formed due to bubble eruption. In the system studied here, the bubbles were approximately 20 mm in diameter, making the entry length approximately 5-10 bubble diameters. This entry length is slightly less than the transport disengaging height of 12 bubble diameters proposed by Hamdullahpur and MacKay (Hamdullahpur and MacKay, 1986) based on theory and experimental evidence. In

order to make conclusions on the possible relation between length required for the decay of a toroidal vortex and other important entry lengths, it is necessary to conduct further experiments similar to those presented here with a variety of different bed diameters, bubble sizes, gases, particles and Reynolds numbers and at higher spatial resolutions to better define the transition to fully developed turbulent flow. Using poppy seeds of different diameters would likely lead to different bubble sizes, and thus conducting analogous experiments with smaller poppy seeds is a logical next step for extending the insights from this study.

5. Conclusions

This work demonstrates the first direct measurements of gas flow patterns in the freeboard of a fluidized bed using magnetic resonance imaging. The gas velocity measurements were demonstrated to be quantitatively accurate, when compared with the average gas velocity measured by a thermal mass flow controller. The results indicated that just above the top surface of the bubbling fluidized bed used, the highest velocity was observed at the walls, with low velocities in the centre of the bed where the bubbles erupted. These results are consistent with the toroidal vortex theory (Levy and Lockwood, 1983) for gas flow patterns in the freeboard above bubbling fluidized beds. The results agree with previous research on the motion of gas and solids in the freeboard using LDA, PIV and PLIF measurements (Duursma et al., 2001; Hartung et al., 2008; Müller et al., 2009; Solimene et al., 2007; Yórquez-Ramírez and Duursma, 2001). It remains a future area of research to determine how this pattern is altered in wider beds in which bubbles erupt at different locations and multiple bubbles can erupt at the same time.

Acknowledgment

CMB acknowledges the Gates Cambridge Trust for funding his research.

Notation

Latin Characters

D_{bed}	Bed diameter
d_p	Particle diameter
H	Expanded bed height
H_0	Tapped bed height
Re	Reynolds number: $(D_{bed}\rho_g U)/\mu$
U	Superficial velocity
U_{mf}	Minimum fluidization velocity
z	Height above the distributor

Greek Characters

μ	Gas viscosity
ρ_g	Gas density

References:

Boyce, C.M., Rice, N.P., Davidson, J.F., Sederman, A.J., Gladden, L.F., Dennis, J.S., Holland, D.J., 2015a. A magnetic resonance study of gas and particle dynamics in a fluidized bed. Science Submitted.

Boyce, C.M., Rice, N.P., Sederman, A.J., Dennis, J.S., Holland, D.J., 2015b. 11-interval PFG pulse sequence for accurate measurement of gas velocity in granular materials. J. Magn. Reson. (submitted).

Callaghan, P.T., 1991. Principles of nuclear magnetic resonance microscopy, books.google.com. Clarendon Press, Oxford.

Davidson, J.F., 1961. Symposium on fluidization – Discussion. Trans Inst Chem Eng 39, 230–232.

Duursma, G.., Glass, D.., Rix, S.J.., Yorquez-Ramirez, M.., 2001. PIV investigations of flow structures in the fluidised bed freeboard region. Powder Technol. 120, 2–11. doi:10.1016/S0032-5910(01)00340-0

Geldart, D., 1973. Types of Gas Fluidization. Powder Technol. 7, 285–292.

Grace, J.R., 1986. Contacting modes and behaviour classification of gas—solid and other two-phase suspensions. Can. J. Chem. Eng. 64, 353–363.

Hamdullahpur, F., MacKay, G.D.M., 1986. Two-phase flow behavior in the freeboard of a gas-fluidized bed. AIChE J. 32, 2047–2055. doi:10.1002/aic.690321215

Hartung, G., Müller, C.R., Hult, J., Dennis, J.S., Kaminski, C.F., 2008. Laser Diagnostic Investigation of the Bubble Eruption Patterns in the Freeboard of Fluidized Beds. 1.

Optimization of Acetone Planar Laser Induced Fluorescence Measurements. Ind. Eng. Chem. Res. 47, 5686–5697. doi:10.1021/ie0713543
Holland, D.J., Gladden, L.F., Müller, C.R., Dennis, J.S., Sederman, A.J., 2008. Spatially resolved measurement of anisotropic granular temperature in gas-fluidized beds. Powder Technol. 182, 171–181. doi:10.1016/j.powtec.2007.06.030
Levy, Y., Lockwood, F.C., 1983. Laser doppler measurements of flow in freeboard of a fluidized bed. AIChE J. 29, 889–895. doi:10.1002/aic.690290603
Levy, Y., Lockwood, F.C., n.d. Laser doppler measurements of flow in freeboard of a fluidized bed. AIChE J. 29, 889–895. doi:10.1002/aic.690290603
Müller, C.R., Hartung, G., Hult, J., Dennis, J.S., Kaminski, C.F., 2009. Laser diagnostic investigation of the bubble eruption patterns in the freeboard of fluidized beds: Simultaneous acetone PLIF and stereoscopic PIV measurements. AIChE J. 55, 1369–1382. doi:10.1002/aic.11802
Pemberton, S.T., Davidson, J.F., 1984. Turbulence in the freeboard of a gas-fluidised bed: The significance of ghost bubbles. Chem. Eng. Sci. 39, 829–840. doi:10.1016/0009-2509(84)85052-6
Solimene, R., Marzocchella, A., Ragucci, R., Salatino, P., 2007. Laser diagnostics of hydrodynamics and gas-mixing induced by bubble bursting at the surface of gas-fluidized beds. Chem. Eng. Sci. 62, 94–108. doi:10.1016/j.ces.2006.08.007
Yang, W.-C., 2007. Modification and re-interpretation of Geldart's classification of powders. Powder Technol. 171, 69–74. doi:10.1016/j.powtec.2006.08.024
Yórquez-Ramírez, M.., Duursma, G.., 2001. Insights into the instantaneous freeboard flow above a bubbling fluidised bed. Powder Technol. 116, 76–84. doi:10.1016/S0032-5910(00)00368-5
Zenz, F.A., Weil, N.A., 1958. A theoretical-empirical approach to the mechanism of particle entrainment from fluidized beds. AIChE J. 4, 472–479. doi:10.1002/aic.690040417

Figures:

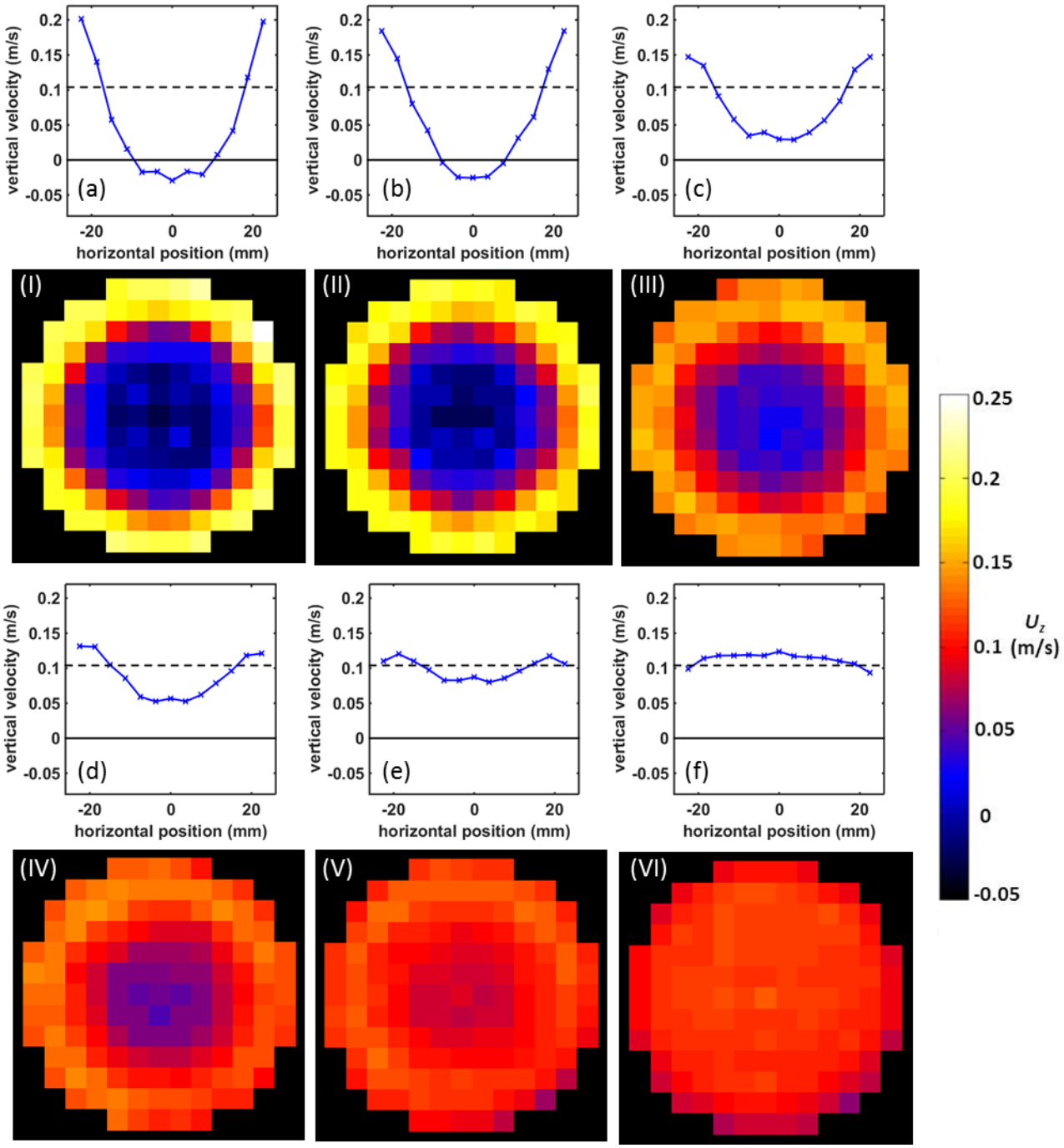

Figure 1 Time-averaged maps of velocity of gaseous SF_6 at different vertical positions in the freeboard region above the fluidized bed. The bed was in the bubbling fluidization regime, *Re* = 18,900, *U* = 0.104 m/s (U_{mf} = 0.090 m/s); field-of-view: 56 mm (*x*) by 56 mm (*y*); slice thickness: 4 mm (*z*); resolution: 3.75 mm (*x*) by 3.75 mm (*y*). The images show maps and graphs show the velocity profile along the centreline of the bed at vertical positions above the expanded bed height of (a) and (I) *z* – *H* = 10 mm, (b) and (II) *z* – *H* = 30 mm, (c) and (III) *z* – *H* = 50 mm, (d) and (IV) *z* – *H* 70 mm, (e) and (V) *z* - *H* = 90 mm, (f) and (VI) *z* - *H* = 180 mm.

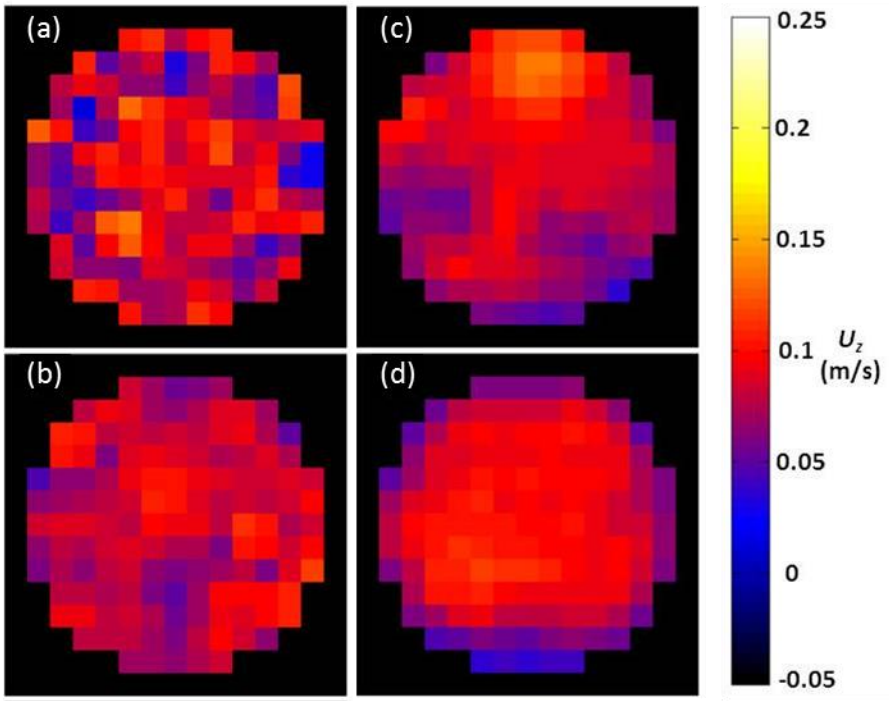

Figure 2 Time-averaged maps of velocity of gaseous SF_6 at different vertical positions in the freeboard region above a bed held at U = 0.080 m/s, just below minimum fluidization U_{mf} = 0.090 m/s. Maps correspond to vertical positions above the expanded bed height of (a) $z - H$ = 10 mm, (b) $z - H$ = 50 mm, (c) $z - H$ = 90 mm, and (d) $z - H$ = 180 mm. The field-of-view was 56 mm (x) by 56 mm (y); slice thickness was 4 mm (z); resolution was 3.75 mm (x) by 3.75 mm (y); Re = 14,600.

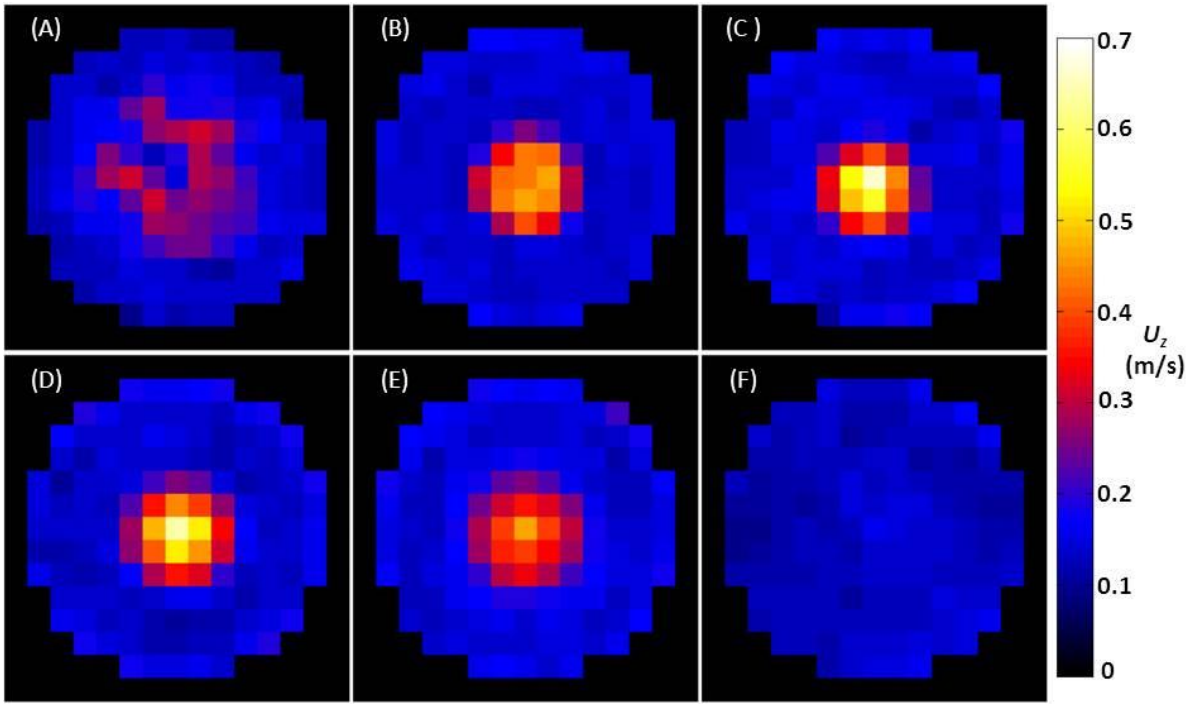

Figure 3 Maps of time-averaged gas velocity of SF_6 at different vertical positions in the fluidized bed of particles. Fluidization regime: bubbling; U = 0.104 m/s; field-of-view: 56 mm (x) by 56 mm (y); slice thickness: 4 mm (z); resolution: 3.75 mm (x) by 3.75 mm (y); vertical positions above distributor: (A) z = 10 mm, (B) z = 25 mm, (C) z = 50 mm, (D) z = 75 mm, (E) z = 100 mm, (F) z = 120 mm (i.e. at the expanded bed height, as determined from imaging of the particles).

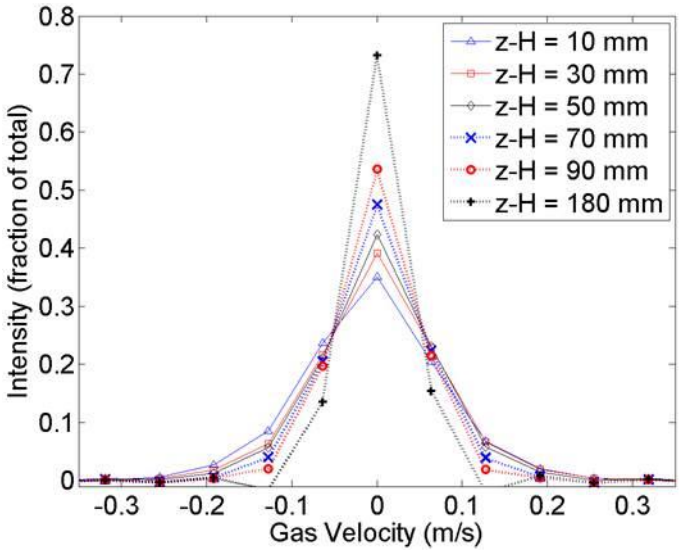

Figure 4 Distribution of the *y*-component of the velocity of SF_6 at vertical positions above the expanded bed height between 10 mm and 180 mm, as indicated. These results were obtained from propagator measurements (Callaghan, 1991). Fluidizing regime: bubbling; U = 0.104 m/s; resolution: 0.0625 m/s; slice thickness: 4 mm (z).

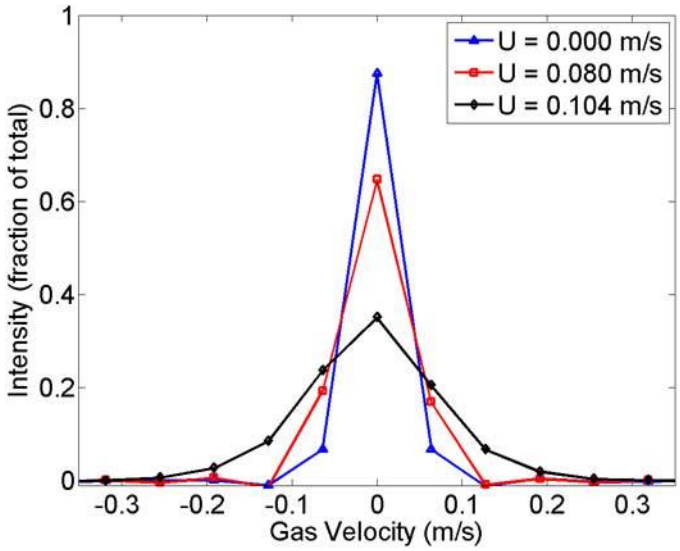

Figure 5 Distribution of the *y*-component of the velocity of SF_6 at superficial velocities corresponding to zero flow, just below minimum fluidization (U = 0.080 m/s) and bubbling fluidization (U = 0.104 m/s). The results were obtained using propagator measurements (Callaghan, 1991) and were recorded at a distance above the expanded bed height: $z - H$ = 10 mm; resolution: 0.0625 m/s; slice thickness: 4 mm (z).

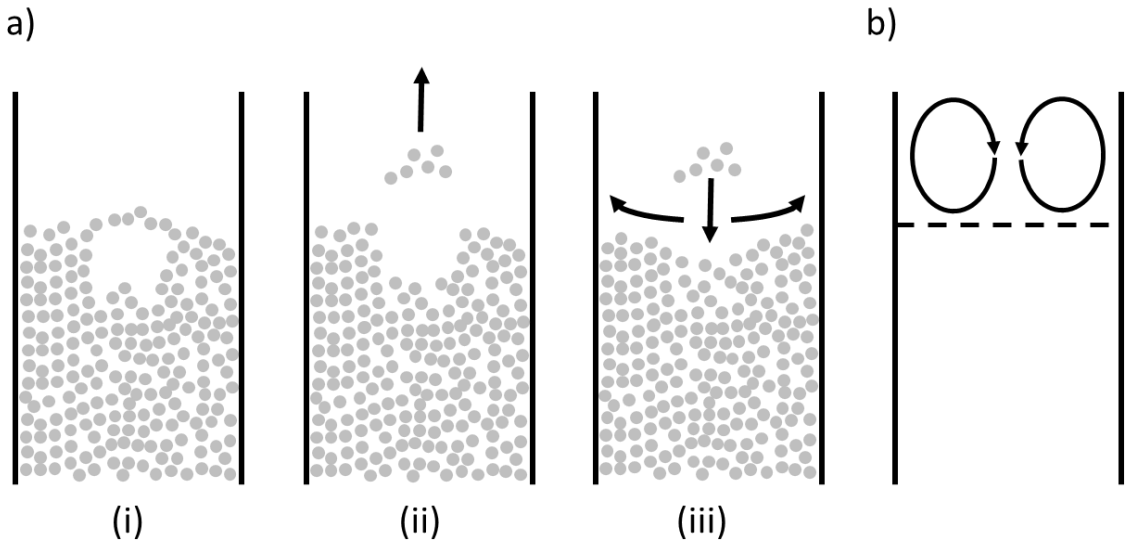

Figure 6 Toroidal vortex formed in freeboard due to bubble eruption: (a) mechanism for vortex formation and (b) shape of the vortex. This figure has been adapted from Hartung et al. (Hartung et al., 2008).

Tables:

Table 1 Fluidized bed properties

Bed Property	Value
Inner diameter (D_{bed})	52 mm
Tapped bed height (H_0)	100 mm
Particle type	Poppy seeds
Particle diameter (d_p)	1.1 mm
Particle density	1040 kg/m^3
Geldart (1973) Grouping	D
Grace (1986) and Yang (2007) Grouping	D
Gas molecule	SF_6
Pressure	7.5 barg
Temperature	25±3 °C
Gas density	56 kg/m^3
Gas viscosity	16 μPa s
U_{mf}	0.090 m/s
U_{mb}	0.090 m/s
Distributor type	Porous bronze plate

Table 2 Parameters for spatially-resolved maps of gas velocity

Parameter	Value
Field of view (FoV)	60 mm (x) by 60 mm (y)
Slice thickness	4 mm (z)
Resolution	3.75 mm (x) by 3.75 mm (y)
Pulse sequence	11-interval
Phase cycling	12-step cogwheel
Observation time (Δ)	6 ms
Flow encoding gradient period (δ)	100 μs
Echo time (τ)	360 μs
Field of flow (FoF)	3 m/s
Recycle time (T_R)	75 ms
Number of flow encoding gradients	3
Number of averages (N_{avg})	4 (freeboard), 8 (bed of particles)
Acquisition time	40 minutes (freeboard), 80 minutes (bed of particles)

Table 3 Vertical positions in freeboard for gas velocity maps

Position	Vertical distance above the expanded bed height, z-H (mm)
I	10
II	30
III	50
IV	70
V	90
VI	180

Table 4 Parameters for measurements of distributions of the horizontal (y) component of gas velocity averaged over the horizontal cross-section of the fluidized bed.

Parameter	Value for *y*-direction propagators
Field of flow (*FoF*)	2.00 m/s
slice thickness	4 mm (z)
Velocity Resolution	0.0625 m/s
Pulse sequence	11-interval
Phase cycling	12-step cogwheel
Observation time (Δ)	30 ms
Flow encoding gradient period (δ)	100 μs
Echo time (τ)	360 μs
Recycle time (T_R)	75 ms
Number of flow encoding gradients	16
Number of averages (N_{avg})	64
Acquisition time	38 min

Table 5 Average velocity measurements from spatially-resolved maps with the 11-interval pulse sequence in the freeboard

Vertical distance above the expanded bed height, *z*-*H* (mm)	Superficial velocity, *U* (m/s)	Average velocity from the 11-interval velocity image (m/s)
10	0.104 ± 0.002	0.102 ± 0.002
30	0.104 ± 0.002	0.103 ± 0.002
50	0.104 ± 0.002	0.105 ± 0.002
70	0.104 ± 0.002	0.104 ± 0.002
90	0.104 ± 0.002	0.105 ± 0.002
180	0.104 ± 0.002	0.105 ± 0.002
10	0.080 ± 0.002	0.081 ± 0.002
50	0.080 ± 0.002	0.081 ± 0.002
90	0.080 ± 0.002	0.082 ± 0.002
180	0.080 ± 0.002	0.082 ± 0.002